PUBLICATIONS OF THE ASTRONOMICAL SOCIETY OF THE PACIFIC, 112:555–565, 2000 April

Michelson Interferometry with the Keck I Telescope

P. G. TUTHILL,[1,2] J. D. MONNIER,[2,3] W. C. DANCHI,[3] E. H. WISHNOW,[3,4] AND C. A. HANIFF[5]

Received 1999 November 29; accepted 1999 December 23

ABSTRACT. We report the first use of Michelson interferometry on the Keck I telescope for diffraction-limited imaging in the near-infrared *JHKL* bands. By using an aperture mask located close to the f/25 secondary, the 10 m Keck primary mirror was transformed into a separate-element, multiple-aperture interferometer. This has allowed diffraction-limited imaging of a large number of bright astrophysical targets, including the geometrically complex dust envelopes around a number of evolved stars. The successful restoration of these images, with dynamic ranges in excess of 200:1, highlights the significant capabilities of sparse aperture imaging as compared with more conventional filled-pupil speckle imaging for the class of bright targets considered here. In particular, the enhancement of the signal-to-noise ratio of the Fourier data, precipitated by the reduction in atmospheric noise, allows high-fidelity imaging of complex sources with small numbers of short-exposure images relative to speckle. Multiepoch measurements confirm the reliability of this imaging technique, and our whole data set provides a powerful demonstration of the capabilities of aperture-masking methods when utilized with the current generation of large-aperture telescopes. The relationship between these new results and recent advances in interferometry and adaptive optics is briefly discussed.

1. INTRODUCTION

Developments in detector technology and optoelectronic hardware over the past decade have meant that real-time adaptive optical systems have now become a common feature of large ground-based optical and near-infrared telescopes (recent reviews may be found in Bonaccini & Tyson 1998; Hardy 1998; Roddier 1999). However, while adaptive optics has enjoyed considerable recent success, other techniques that utilize postdetection data processing, rather than real-time compensation, have remained valuable for imaging at the very highest angular resolutions. The best known, and most straightforward of these to implement, is speckle imaging (Labeyrie 1970; Weigelt 1991; Negrete-Regagnon 1996), in which sequences of short exposures of a target and an unresolved calibrator are used to recover high-resolution maps beyond the natural seeing limit. Although this method in principle allows the recovery of images of arbitrary complexity, the difficulty of attaining an adequate signal-to-noise ratio (S/N) has meant that it has mainly been confined to studies of binary stars (see, for example, Patience et al. 1998) and other astronomical sources with similarly simple geometries (although Weigelt et al. 1998 is a recent counterexample).

One solution to this S/N problem is to modify the pupil geometry of the telescope using a mask so as to mimic the operation of a separated-element interferometer array such as the Very Long Baseline Array (VLBA). This process can be considered as finding an optimal balance between the level of atmospheric perturbations, the number of photons, and the amount of structural information measured about the source—all of which increase as the pupil area rises. When an aperture mask is being used, the data collection and analysis methods are similar to those utilized for speckle imaging, but with a reduction in the number of independent spatial frequencies measured, which is balanced by an improved S/N on the data which are obtained. This postprocessing approach has been widely exploited at optical wavelengths, where it has established itself as the only method by which reliable images of the surfaces of nearby stars at the diffraction limit have been recovered for ground-based telescopes (see, for example, Buscher et al. 1990; Wilson, Dhillon, & Haniff 1997; Tuthill, Haniff, & Baldwin 1999a).

In this paper, we report the first aperture-masking experiments to exploit the new generation of 10 m class telescopes.

[1] Current address: Chatterton Astronomy Department, School of Physics, University of Sydney, NSW 2006, Australia; gekko@physics.usyd.edu.au.

[2] Current address: Smithsonian Astrophysical Observatory MS 42, 60 Garden Street, Cambridge, MA 02138; jmonnier@cfa.harvard.edu.

[3] Space Sciences Laboratory, University of California at Berkeley, Berkeley, CA 94720-7450; wcd@ssl.berkeley.edu, wishnow@ssl.berkeley.edu.

[4] V Division, Lawrence Livermore National Laboratory, 7000 East Avenue, Livermore, CA 94550.

[5] Astrophysics Group, Cavendish Laboratory, Madingley Road, Cambridge, CB3 0HE, England, UK; cah@mrao.cam.ac.uk.

We have used the Keck I telescope with a variety of sparse multiaperture pupil masks both to verify the S/N and calibration advantages of these pupil geometries and to demonstrate the ability of this method to provide diffraction-limited imaging of resolved targets in the near-infrared with excellent dynamic range. We have used multi-epoch measurements to establish the reliability of our imaging, and we present near-infrared maps of the highly structured dust shells of a number of evolved stars at resolutions exceeding 50 mas.

2. EXPERIMENTAL DESIGN

Aperture masking and conventional speckle interferometry share much in common, including the ultimate goal of recovering the complex visibility function of the target of interest (i.e., the Fourier transform of its brightness distribution) at all spatial frequencies up to the telescope diffraction limit. Generally, although Fourier amplitudes can be measured (Fizeau 1868; Michelson 1890), phases are scrambled by the atmosphere, necessitating the use of an observable known as the closure phase (Jennison 1958). More recently, closure phase concepts have been generalized into the mathematical formalism of bispectral or triple correlation analysis (Lohmann, Weigelt, & Wirnitzer 1983).

Apart from the mask itself, the instrumental setup required for masking is almost identical to that for speckle, with sequences of short-exposure data frames being recorded at high magnification, allowing for the image degradation caused by atmospheric turbulence to be removed during postprocessing. The principal difference between the two types of experiments is that in aperture masking the pupil geometry can be adjusted to optimize the S/N. The implementation of a masking interferometer at the Keck I telescope is discussed in more detail in the following sections.

2.1. Optical Setup

Unlike most earlier aperture-masking experiments (e.g., Haniff et al. 1987; Readhead et al. 1988), which used screens placed in a small reimaged pupil, masking of the Keck primary was achieved by placing large (30 cm on a side hexagonal) aluminum masks directly in front of the f/25 infrared secondary mirror as shown in Figure 1. At this location, beams propagating to the detector are sufficiently well separated that masks can be treated as selecting discrete portions of the pupil, despite this not being a true pupil plane. With this design, however, the masks intercept radiation from the source twice: once on the way from the primary to the secondary, and a second time when traveling back toward the detector. As a consequence, masks selecting N subapertures on the primary mirror in principle require $2N$ holes. In order to accommodate this double pass correctly, ray-tracing software was used to confirm that rays passing through each subaperture could indeed be

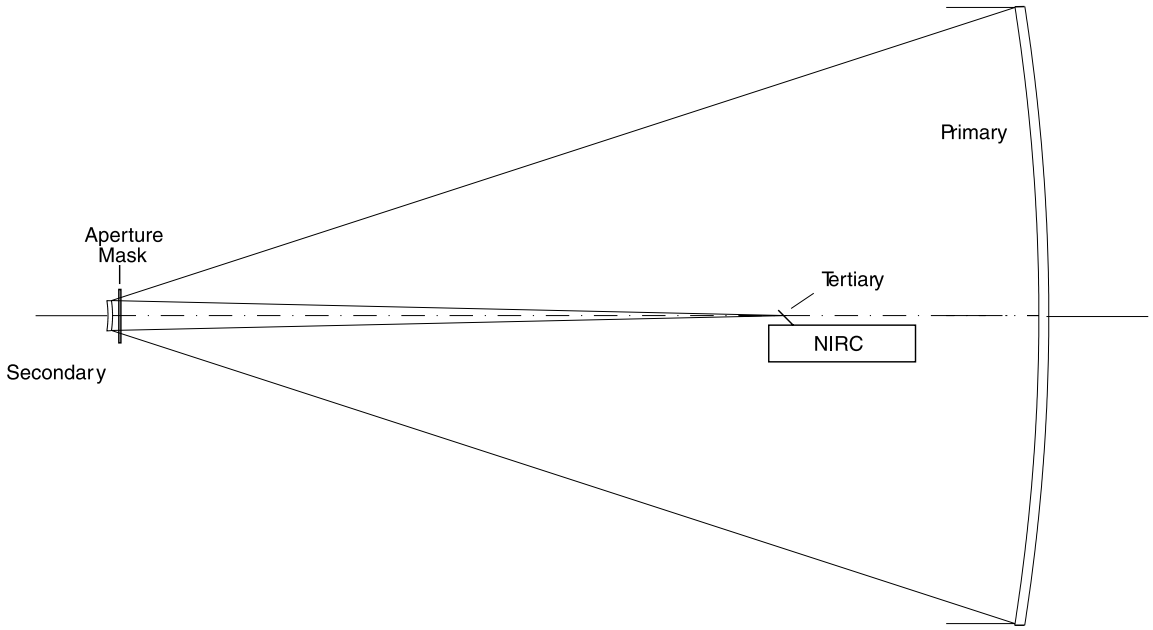

FIG. 1.—Optical ray trace of starlight from the primary mirror of the Keck telescope (*right*) to the NIRC. Aperture masks placed in front of the secondary mirror as shown must be designed to take into account complications arising from the double light path and the effects of the converging beam at this point in the optical train.

traced back to discrete regions on the primary mirror. The masks were fabricated of 3/16 inch aluminum sheet and were mounted on a custom-built cylindrical post that protruded through the central hole of the f/25 secondary. At this location, the masks could be accessed during the night, permitting changes from one mask to another to optimize the configuration for a given source (this swap procedure took approximately 10 minutes). A typical desired pupil shape and the mask required to implement it are shown in Figure 2.

After passing through the mask, the beams were focused on the Keck facility Near Infrared Camera (NIRC), using external magnifying optics (the so-called image converter; Matthews et al. 1996). The plate scale was 20.57 mas pixel^{-1} on the 256 × 256 pixel InSb array, sufficient to Nyquist sample data collected in the K band or longer wavelength bands. The observing wavelengths were selected from NIRC's standard complement of interference filters which offered a range of bandwidths (1%–20%) covering the 1–3.5 μm region.

Although the masks were not cooled, this had little impact on the experiment. At wavelengths shorter than the K band, the fast exposures (typically 140 ms or less) ensured that there was little contribution from thermal emission. At longer wavelengths, thermal emission from the masks should have been a significant factor. However, the masks produced only a negligible increase in the thermal background, primarily because of the design of the NIRC magnifying optics. Because NIRC contains only a single cooled Lyot stop, when the image converter (Matthews et al. 1996) is in use, the cold stop is significantly oversized. The array is exposed to room-temperature radiation (mostly from baffles and other camera structures), so the presence of the masks had little effect on the thermal background, which was already dominated by ambient flux.

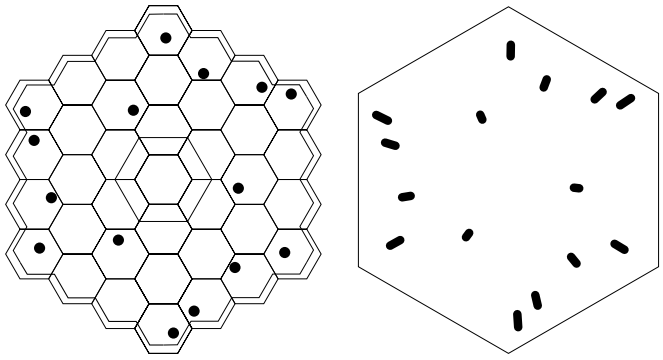

FIG. 2.—Desired sparse pupil (*left*) and the aperture mask used to generate it (*right*). The required pupil is shown as the set of black spots and is superimposed on a scaled version of the segmented 10 m Keck primary mirror (hexagonal segments). The boundary of the undersized f/25 secondary mirror as projected on the telescope primary is represented as the bold black line. The right-hand panel shows the corresponding aperture mask, ray-traced for a location 60 mm from the pole of the secondary mirror. In this case the elongated apertures allow the light to traverse both to and from the secondary on its way to the detector. The hexagonal mask plate is 300 mm on a side. The central mounting hole for the mask is not shown in this figure.

2.2. Mask Design

Most pupil mask designs used nonredundant configurations of subapertures, each with an effective size when projected onto the primary mirror of 20–35 cm. This was tailored to be of order the seeing scale size, r_0. The lack of redundancy ensured that any Fourier component measured could be uniquely identified with a particular pair of subapertures, while the small sizes minimized the effects of wave front perturbations across each subaperture (<1 radian rms). However, the segmented nature of the Keck primary mirror and the undersized infrared secondary significantly complicated the task of locating the subapertures. In particular, when designing the masks, geometries where subapertures were crossed by the telescope spider or panel boundaries in the segmented primary mirror had to be avoided where possible. Designs were also driven by the desire that snapshot Fourier plane coverage be uniform and isotropic. The specific nature of these constraints meant that it was not possible to exploit the results of Keto (1997) or Cornwell (1988), both of whom explored optimum snapshot array configurations for radio interferometers.

Mask designs were based on the approach of Golay (1970), in which threefold symmetric spaces were searched for nonredundant array solutions with compact and dense u-v coverage. Examples of arrays developed for 15 and 21 hole masks are shown in Figures 2 and 3. As can be seen in the 21 hole mask, the Fourier plane coverage has a densely filled core out to baselines of approximately 3 m, and then adequate, but not isotropic, coverage out to the edge of the telescope pupil. Solutions with numbers of apertures as large as 36 were found, but for many experiments a 21 hole mask was more than adequate: this allowed the simultaneous measurement of 210 baselines and 1330 closure phases, yielding an excellent snapshot imaging capability.

Apart from defining the spatial frequencies measured by the telescope, the aperture mask also served to limit the total amount of flux collected. For observations of bright sources (M supergiants and Mira variables can have K magnitudes as high as -4 mag) this was an important feature, as the use of the unobscured pupil would have saturated NIRC in a small fraction of the minimum available exposure time, despite the use of the narrowest available filters.

For dimmer sources, nonredundant masks such as those described above did not transmit enough flux to overcome the array readout noise. The use of partially redundant annular masks, as suggested by Haniff & Buscher (1992), provides continuous Fourier plane coverage and enhanced throughput at the expense of only twofold redundancy. This

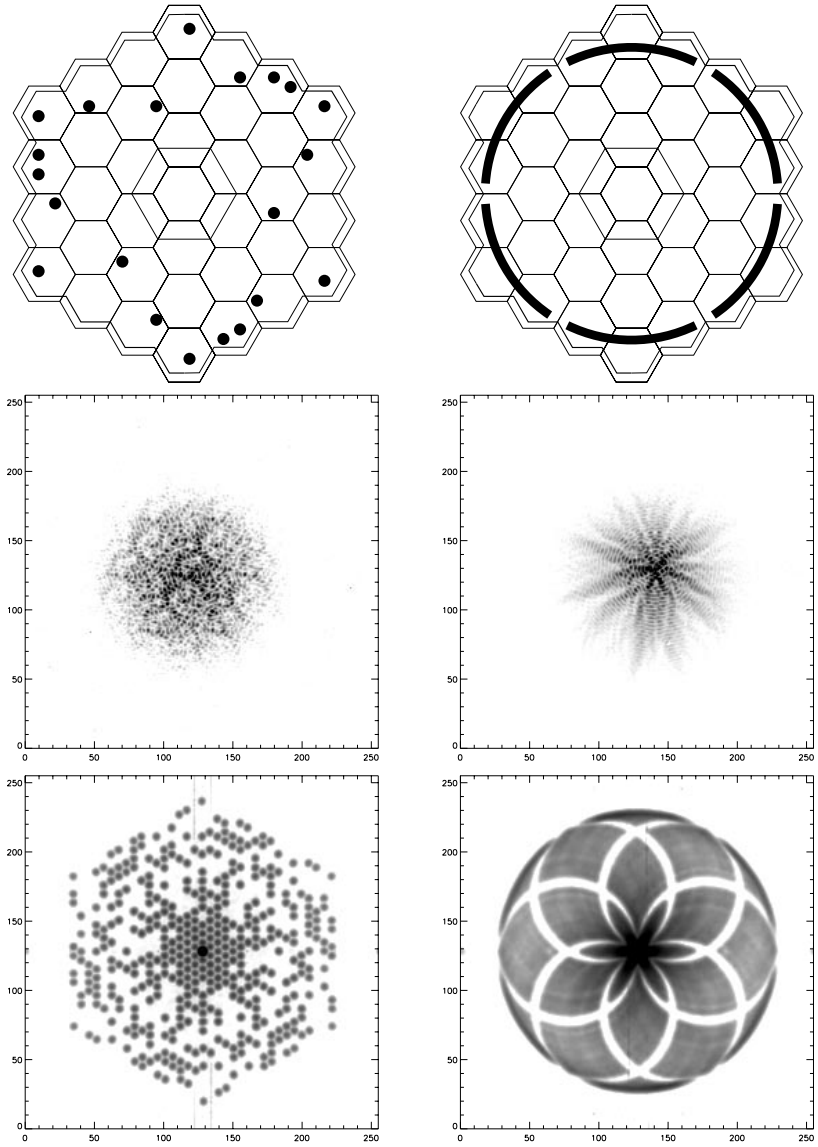

FIG. 3.—Aperture configurations (*top*), single-exposure interferograms (*middle*), and accumulated power spectra of 100 exposures (*bottom*) for two different mask geometries. Each mask is shown superimposed on the Keck primary. Dark regions in the accumulated power spectra reveal the spatial frequencies sampled by each pupil. In the case of the 21 hole Golay mask (*left panels*), the Fourier coverage is confined to a set of 210 independent frequencies, whereas the annular mask (*right panels*) gives quasi-complete coverage within a circular boundary.

approach has been adopted here. An example of such a mask with a throughput of approximately 10% is shown in Figure 3, together with a short-exposure interferogram and its power spectrum. For sources with K magnitudes fainter than about 4 mag, the S/N from masking interferometry was dominated by readout noise, undermining the advantages offered by sparse pupils and necessitating the use of the full pupil.

One unusual feature of our nonredundant Golay masks is that they allowed measurements of interference fringes that were sub-Nyquist sampled. As mentioned in § 2.1, the pixel scale of NIRC only allowed for Nyquist sampling of the longest available baselines at wavelengths greater than 2 μm. At shorter wavelengths, power at the corresponding spatial frequencies is "aliased" back into the power spectrum at lower spatial frequencies, and in most experiments, this signal will overlap and become confused with other shorter baseline signals. With the sparse pupils used here, however, these aliased signals were often mapped back onto otherwise unsampled frequencies and so measurements of the long-baseline interference signals could still be made. In practice, the undersampling attenuated the signals significantly, and the recovery of useful data was only possible in cases where the S/N was initially very high. Nevertheless, we have used this device to recover the J-band visibility functions of a handful of the brightest supergiants and Mira

variables at the highest spatial frequencies where the fringes were sub-Nyquist sampled.

3. OBSERVING PROCEDURE

In view of the close relationship between aperture masking and conventional filled-aperture speckle interferometry, observations were secured using a schedule very similar to that used in other high-resolution imaging experiments (see, e.g., Matthews et al. 1996). For each target 100 short-exposure interferograms were collected, after which a smaller number (usually 10) of identical exposures were secured on nearby blank sky. The exposure times were limited by the array readout, with times of 140 ms possible for the full 256 × 256 NIRC array. This is longer than the typical atmospheric coherence time (t_0) expected at 2.2 μm ($\sim$40 ms), resulting in added atmospheric noise for the bispectral measurements. However, integration times of a few t_0 preserve significant fringe power and actually deliver higher S/N in the photon-noise–limited (faint source) regime (Buscher 1988), while the closure phase is even more robust and can be measured with integrations of many t_0 (Readhead et al. 1988). Shorter exposure times could be obtained by reading out smaller subframes of the array, but in general the large sizes of the interferograms, resulting from the small dimensions of the pupil subapertures, meant that subframing was problematic for reasons of data calibration and loss of field of view.

Calibration of the mean telescope-atmosphere transfer function was performed by interleaving the 100 source plus 10 sky data sets with identical exposures of nearby similarly bright calibrator stars. Sets of these "matched pairs" of data were secured for each source and wavelength of interest, giving a total elapsed time for each complete observation of order 10 minutes. Currently this time remains limited by the $\sim$10% duty cycle of the real-time archiving software available at NIRC, which was not designed with this mode of operation in mind: custom-designed hardware would likely increase the data collection rate by an order of magnitude. Despite the low duty cycle of the camera, the use of nonredundant pupils allowed high S/N image reconstructions of resolved targets to be achieved with relatively small numbers of specklegrams (i.e., as few as a hundred). This should be contrasted with the thousands typically used in filled-aperture speckle experiments, where the atmospheric redundancy noise limits the S/N per frame of the Fourier measurements to unity even at high light levels.

Where possible, filter bandpasses of $\lesssim$5% were used in order to minimize the effects of the expected differences in spectral type between the targets and their calibrator stars. Without such precautions, the differing spectral shapes over the bandpass could affect the calibrated data. The most interesting sources—those with suspected well-resolved structure—were observed at two well-separated times during the night. This allowed independent checks to be made on the reliability of source structure determinations since spurious signals associated with the mask and detector array are not expected to rotate with the sky. Additional observations were also secured each night of a number of binary stars with well-determined orbits to allow independent calibration of the detector orientation and scale and to assess the reliability of the subsequent data reduction pipeline.

4. DATA REDUCTION

Analysis of the data followed standard methods for aperture-masking experiments and involved the accumulation of the power spectra and bispectra of each set of interferograms. As a first step, each short-exposure image was dark-subtracted, flat-fielded, and cleaned of pattern noise arising from transients in the readout electronics and variations in the behavior of the four different readout amplifiers. Images were subsequently windowed with a two-dimensional Hanning function tapered to zero so as to eliminate edge effects. Power spectra could now be computed frame by frame from the squared modulus of the Fourier transform. Stellar fringe signals appeared as power at discrete locations in such spectra, with the origin occupied by a peak whose height was proportional to the squared flux in the frame, while the remaining areas were filled with a signal caused by a combination of photon and readout noise (for illustration, see Fig. 3).

The noise power level, which would otherwise bias the measurements, could be obtained by averaging over those regions where no stellar signal was expected (usually, but not always, at the edges of the power spectra). Having subtracted off the noise bias, squared visibilities (Fourier amplitudes) for the stellar interference signal were found by taking the ratio of the power at the spatial frequency of the fringes to the power at the origin and then normalizing with the corresponding signal from the calibrator spectrum. Error estimates were derived from the spread in values amongst each ensemble of 100 exposures. Some typical results from this procedure are shown in Figure 4.

Fourier triple products, or bispectral data, could also be computed for each frame. Closure phase information was recovered from the argument of the complex bispectral data accumulated over the ensembles of short exposures. Again the measured closure phases for the reference stars were used to calibrate the measurements of the targets; however, such corrections, indicative of optical aberrations in the telescope/camera, were small ($\lesssim$few degrees). Unlike filled-aperture speckle experiments, the use of an aperture mask ensured that only a very small subset of the full bispectral hypervolume needed to be accumulated, dramatically

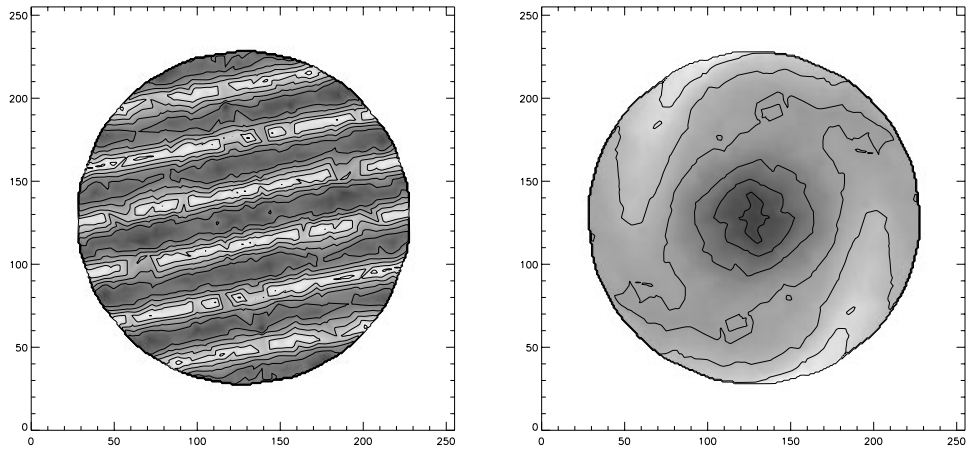

FIG. 4.—Examples of calibrated visibilities recovered from annular mask data. Axes show the spatial frequency (UV) plane, with zero spatial frequency translated to the center, while the boundaries of the figures are at the Nyquist sampling limit. Note that the measurements have been interpolated to fill the Fourier plane and so do not show the gaps in the Fourier plane coverage not sampled by the mask. The data in the left-hand panel are for the binary star α Com and clearly display the expected sinusoidal modulations in visibility. The right-hand panel shows the visibility function of the dusty Wolf-Rayet star WR 104, a more resolved target with a large asymmetric near-infrared envelope.

reducing computational and data storage requirements. A standard workstation was adequate for all data processing.

Having obtained sets of calibrated Fourier amplitudes and closure phases, diffraction-limited images were recovered using standard radio astronomical self-calibration methods. These techniques, originally developed for dilute phase-unstable radio arrays such as the VLBA, are readily transferable to this application since our data, i.e., sampled Fourier amplitudes and closure phases, are almost identical to those delivered by arrays such as the VLBA. The imaging results reported here were obtained using a "maximum entropy method" based implementation of self-calibration (Gull & Skilling 1984; Sivia 1987), but in all cases reconstructions from CLEAN-based methods (Högbom 1974) gave similar results. In many instances the extraction of quantitative information was achieved in a more robust and precise fashion from model fitting directly to the Fourier data than from mapping, particularly when source structure was relatively simple and/or partially resolved.

5. WAVE FRONT COHERENCE

Since the success of interferometric imaging is critically dependent on the coherence properties of the incoming wave front, experiments such as the ones reported here can in principle yield valuable information on the stability and aberrations introduced by mechanical deformation of the telescope and by fluctuations in the atmosphere. The former of these is particularly relevant in consideration of the performance of the segmented primary mirror. Quantitative investigations require a numerical simulation of the phase irregularities introduced by both the atmosphere and telescope pupil. Although we have performed such computations, a full discussion of this work lies beyond the scope of the present report. Instead, a number of general conclusions and difficulties experienced, some of which may be peculiar to the Keck, are outlined below.

The most obvious manifestation of optical aberrations related to the segmented primary is the loss of spectral power (or fringe visibility), implying decorrelation of the wave fronts, at spatial frequencies which can be traced back to the locations of the edges of the hexagonal primary panels. This effect, sometimes referred to as "print-through" from the segmented pattern which appears in the power spectra, has also been seen by workers undertaking full-pupil speckle observations (A. M. Ghez 1997, private communication). We have studied this effect in two ways. First, numerical simulations involving turbulence-degraded wave fronts have verified that significant phase discontinuities ($\gtrsim 0.5\ \lambda$) at the segment boundaries do indeed result in a loss of spectral power which mimics the observations. Second, experimental confirmation of this effect has been obtained by deliberately displacing selected mirror segments in small increments with respect to their neighbors. The overall finding of these studies is that between 1995 and 1997, the Keck I primary was poorly phased when working in the infrared, with most segment edges exhibiting $\gtrsim 0.5\ \lambda$ phase steps. This can probably be traced to suboptimal performance of the "malign" alignment procedure. In 1997, however, the primary mirror alignment procedures (Troy et al. 1998; Chanan et al. 1998) were refined and since then phase discontinuities, while still present, have been greatly ameliorated.

A further problem we have experienced that is possibly related to the segmented primary concerns the anomalously low visibilities measured at long baselines. Measured point-source visibilities were lower by a factor of 2–3 than the values expected on the basis of numerical simulations. One

likely candidate for this loss is the active control system responsible for maintaining the relative alignment between segments. Significant oscillation or jitter of the system is known to occur (P. Wizinowich 1999, private communication), which perturbs the segments at frequencies of tens of hertz—rapidly enough to blur the fringes and introduce a loss in visibility comparable to that we have observed.

Perhaps most damaging of the limitations encountered was the difficulty in ensuring the intermediate-term ($\sim$10 minutes) stability of the optical transfer function necessary for reliable calibration of the measurements. Miscalibration effects, introduced where there had been a change in the seeing-averaged system transfer function between measurements of source and calibrator, were the major obstacle in recovering high-fidelity image reconstructions. One can envisage many sources of this problem. Without a doubt, changes in the local seeing could have occurred over the $\gtrsim$4 minute time lag between source and calibrator observations. Although the use of an aperture mask is known to limit the sensitivity of spatial interferometry to seeing variations, some miscalibration must be traced to this. Alternatively, any flexure of the telescope structure or changes in the phasing of the primary mirror could contribute to a nonstationary transfer function. In practice, the reference stars used were invariably at different elevations in the sky (worst cases could be greater than 10° away), and inevitable changes in the telescope wind loading and temperature all will have contributed to the difficulty of maintaining tolerances for interferometric observations. Further work to identify and remedy this calibration problem would dramatically enhance the precision of this high spatial resolution experiment.

6. RESULTS AND DISCUSSION

Observing in the near-infrared with the 10 m baselines available at the Keck yields an angular resolution appropriate for large targets. The excellent snapshot Fourier coverage of the telescope provides a densely sampled a stellar visibility function with orders of magnitude greater efficiency than a separated element array with a small number of stations. The ability to secure data rapidly and through a wide range of narrow bandpasses has been particularly useful for investigating the atmospheric structure of cool supergiants. Stellar diameters are common science targets in high angular resolution astrophysics (see, e.g., van Belle et al. 1999 for some recent results). Figure 5 shows the azimuthally averaged visibility function of Betelgeuse (α Ori) at four different wavelengths as measured in 1997 December. Although a uniform disk model appears to be quite a good fit to the data at all the measured wavelengths, the star appears to exhibit an anomalously large diameter at 3.08 μm ($\delta\lambda = 0.10$ μm), probably related to the presence of atomic or molecular absorption within the bandpass changing the optical depth of the stellar atmosphere.

In cases where the sources were significantly resolved, very high quality images could be obtained. Figure 6 shows maps of the binary stars 126 Tau and α Com recovered from 100 interferograms. For both maps the dynamic range achieved, as measured by the ratio of the noise in the map to the peak intensity, was considerably better than 0.5% or 1:200. The nonlinear contour levels in the plots of Figure 6 were chosen to highlight features at the level of the noise. The ultimate limitations to the dynamic range can be traced back to systematic miscalibration of the visibility amplitudes and poor handling of noise on the closure phases by the mapping software. Insufficient Fourier sampling and low signal flux—problems which are exacerbated by the use of a mask—were rarely an important contribution to the mapping error budget.

More powerful arguments for the use of sparse pupil geometries in near-infrared speckle imaging are provided by our results for complex resolved sources. Figure 7 shows two such images of the dust enshrouded carbon star CIT 6 and the IR-bright Wolf-Rayet star WR 104. Both of the sources are clearly resolved at the tens of milliarcsecond scale, and their complex structures, which have been confirmed through independent repeated observations (see, e.g., Tuthill, Monnier, & Danchi 1999b), demonstrate the unique facility that the combination of interferometric methods with the large Keck primary provides. Both maps have dynamic ranges better than 100:1 and are of comparable quality to the images routinely produced by modern radio VLBI arrays. Illustrations of the high level of repeatability for maps taken over separate epochs can be found in Monnier et al. (1999a).

Scientific results from the masking program at Keck have encompassed a range of astronomical topics from measurements of stellar photospheres (e.g., Monnier et al. 1997; Tuthill, Monnier, & Danchi 1998a; Tuthill et al. 2000) to imaging circumstellar dust shells in evolved stars (e.g., Tuthill et al. 1998c; Tuthill, Monnier, & Danchi 1999c; Danchi et al. 1998; Monnier et al. 1999a) and enshrouded Wolf-Rayet stars (Tuthill et al. 1999b, 1999c; Monnier, Tuthill, & Danchi 1999). As is discussed further in Monnier (1999), the parameter space addressed by this experiment—bright objects ($m_k \lesssim 4$ mag) with resolvable structure on 10 m baselines—is a particularly rich one since the combined resolution and magnitude limits are fortuitously matched for targets containing hot astrophysical dust at around $\sim$1000 K. Further discussion of the program stars and techniques may be found in Tuthill et al. (1998b) and Monnier (1999).

In contrast to the situation only decades ago, astronomers are now armed with a number of different techniques all aimed at overcoming the seeing limit in astronomical observations. These include aperture masking, separate-

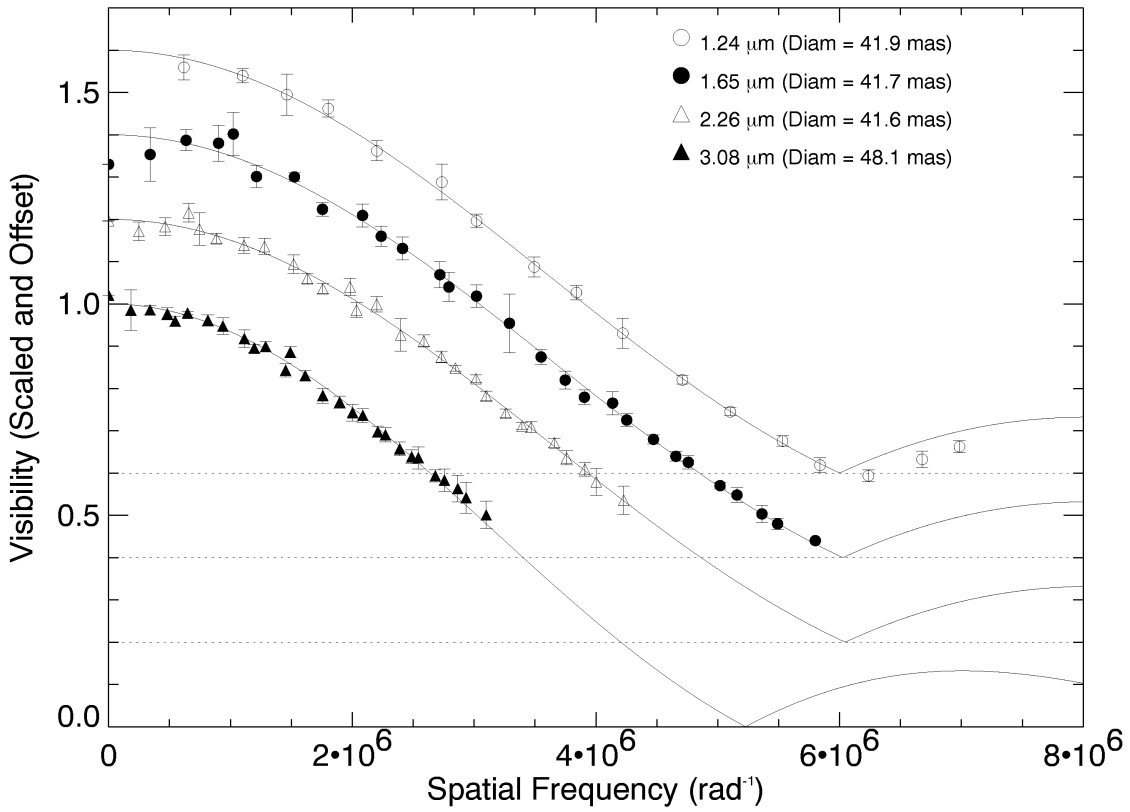

FIG. 5.—Azimuthally averaged visibility amplitudes for Betelgeuse (α Ori) as measured in 1997 December at four different wavelengths. In each case the best-fit uniform disk model (see key for diameters) is shown overplotted as a solid line. To avoid confusion, the data at the different wavelengths have been offset by fixed amounts.

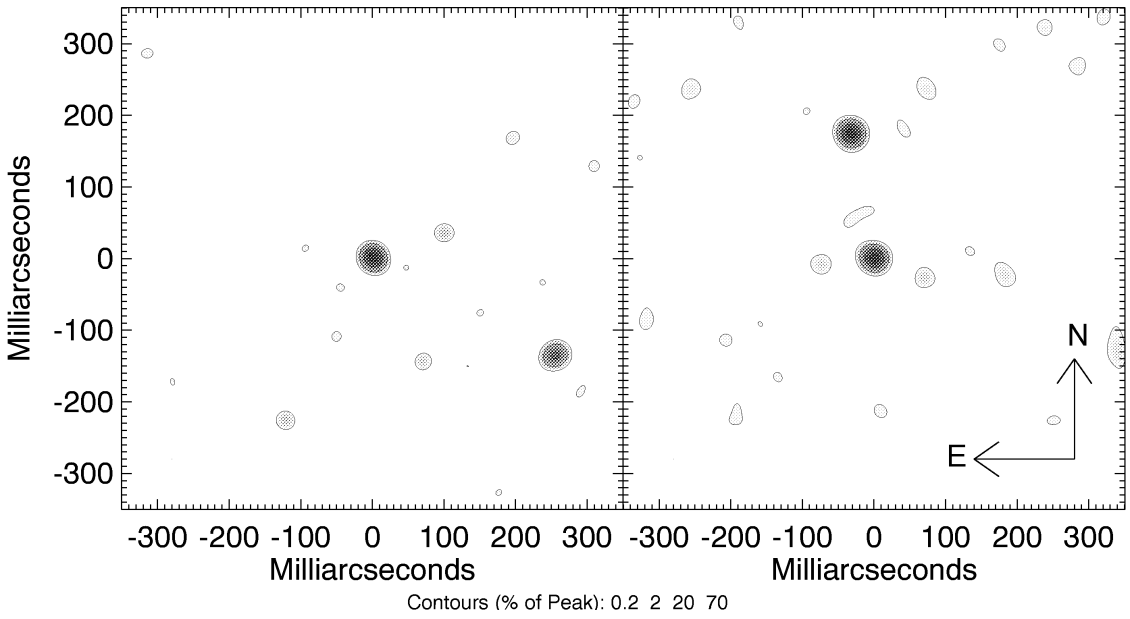

FIG. 6.—Reconstructed *K*-band images of the binary stars 126 Tau (*left*; 1998 September) and α Com (*right*; 1998 April). The logarithmic contour levels, at 0.2%, 2%, 20%, and 70% of the peak, were chosen to highlight the very small noise features in each map. Although the binary separations for these stars are only 287 and 177 mas, respectively, they are easily separated at the diffraction limit of the Keck telescope.

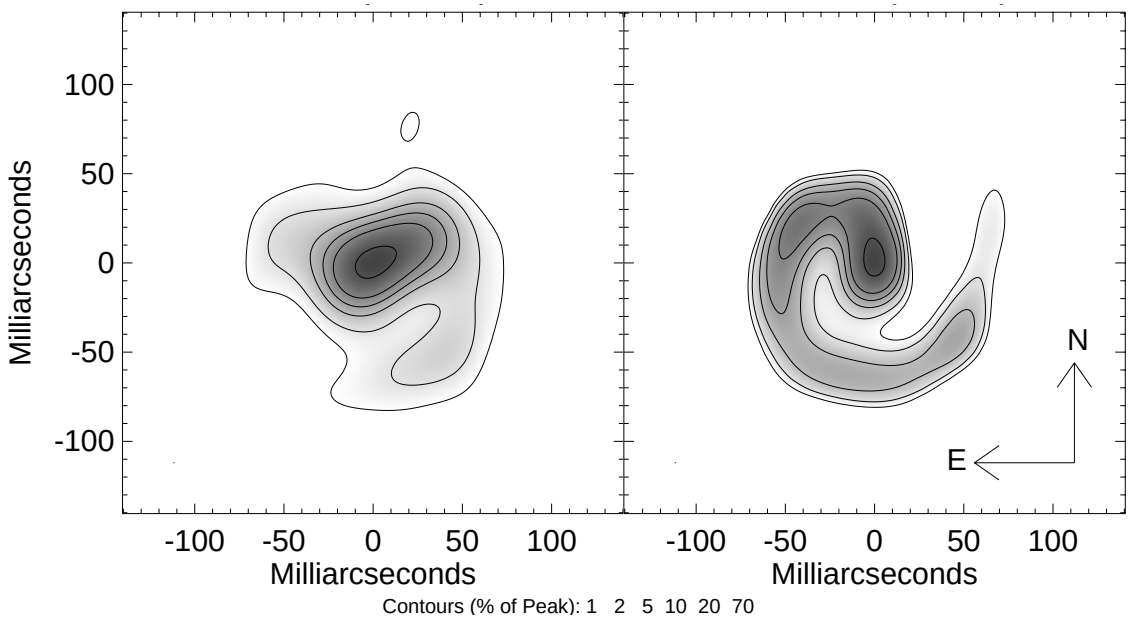

FIG. 7.—Diffraction-limited images of the evolved carbon star CIT 6 (*left*; 1997 December) and the dusty Wolf-Rayet star WR 104 (*right*; 1998 June) reconstructed from *K*-band measurements taken with the 15 hole Golay and annular masks, respectively (see Figs. 2 and 3). For asymmetric objects such as these, the recovery of high-quality phase information is crucial in recovering the true flux distribution.

element interferometry, speckle interferometry, observations from space, and adaptive optics (AO), with the distinctions between these areas becoming increasingly blurred. Nonredundant, or partially redundant, masking occupies a particular niche in this parameter space and has been successful for bright objects resolvable with relatively modest baselines. The primary competing technologies here are speckle interferometry and adaptive optics, which we discuss in turn below.

Although there has been much debate on the relative merits of masking versus speckle interferometry, there is agreement that for the faintest objects (where "faint" is ultimately defined as a small number of photons in a coherent patch per coherence time, but in practice is usually governed by readout noise in the IR array detector before this limit is attained) speckle interferometry is the superior choice. For bright sources, there is little doubt that masking offers dramatic S/N advantages for discrete measurements of Fourier amplitudes and closure phases (e.g., Roddier 1987). However, filled-pupil speckle interferometry is capable of recovering far greater volumes of data, completely filling the bispectral volume, albeit at low S/N. A number of studies have addressed the comparison of nonredundant versus filled pupil from theoretical, numerical simulation, and observational approaches (Readhead et al. 1988; Haniff & Buscher 1992; Buscher & Haniff 1993) and have concluded that there are clear regions where masking can outperform filled-pupil techniques in recovering diffraction limited images of arbitrary celestial objects. In practice, superb images have been recovered using both techniques (for examples of recent speckle images, see Weigelt et al. 1998). A choice of which technique should be used is often also driven by more mundane considerations, which in our case included saturation of the camera on bright stars and the availability of a well-characterized and mature image reconstruction code, both of which favor a masking strategy.

In making a comparison of the relative merits of adaptive optics, a separate set of considerations present themselves. Many of the masking program stars, in addition to being bright, also exhibit a compact core and therefore might be thought ideal targets for natural guide-star adaptive optical systems. However, a strong note of caution needs to be sounded against the optimistic projection that such systems will render postprocessing techniques such as masking or speckle rapidly obsolete. Obtaining true diffraction-limited images from current AO data requires careful deconvolution of the point-spread function (PSF). It has been our experience (Monnier et al. 1999a) that the PSF of an AO system is difficult to fully characterize and, worse, is not stationary when the telescope is moved to a calibration star which will usually be of different brightness, elevation, and spectrum. In his recent review of AO, S. T. Ridgway[6] notes that the problem of erratic PSF artifacts, which can easily masquerade as genuine source structure, is endemic to current-generation AO systems. For all its unappealing

[6] S. T. Ridgway, 1999, Ground Based Astronomy with Adaptive Optics, review obtained on-line at http://www.noao.edu/~ridgway/.

appearance, an uncompensated speckle cloud has the advantage that it results from simpler underlying processes—the atmosphere and telescope optics only—with the result that (in the high-light limit) it is easier to calibrate. We hasten to point out that AO offers numerous and dramatic advantages across a wide spectrum of observational problems (e.g., Ridgway 1999 review); our discussion here is limited only to bright stars with structure at the highest angular resolutions.

7. CONCLUSIONS

Results from the first aperture-masking experiment performed on a 10 m class telescope are presented. A suitable choice of non- or low-redundancy pupil geometries has been found to dramatically improve the S/N on recovered bispectral data. Reliable images with complex and asymmetric structure at the diffraction limit have been routinely produced in the near-infrared *JHKL* bands. With dynamic ranges in excess of 200:1 and demonstrated repeatability of map structure over multiple observing epochs, the expected advantages of sparse-aperture interferometry for bright targets have been confirmed. In a comparison of aperture masking, full-pupil speckle, and adaptive optics, the most reasonable conclusion appears that each technique has regions of the parameter space of source brightness and spatial structure where it offers superior performance. The existence of such complementary observational techniques will certainly be beneficial in addressing a range of problems in high-resolution astronomy, with masking being at its most effective for the brightest objects at the highest angular resolutions. The robust reconstruction of complex brightness distributions from sparsely sampled Fourier data augurs well for the future of the next generation of separate-element ground-based imaging arrays with baselines in excess of an order of magnitude larger than those available here.

The authors would like to thank Gary Chanan and Mitchell Troy for their help with performing the segment phasing experiments. We would also like to thank Everett Lipman, Charles Townes, Peter Gillingham, and Terry McDonald, all of whom have contributed to the success of our endeavors. Devinder Sivia kindly provided the maximum entropy mapping program VLBMEM, which we have used to reconstruct our diffraction limited images. This work has been supported by grants from the National Science Foundation (AST 93-21289 and AST 97-31625). C. A. H. is grateful to the Royal Society for financial support. E. H. W. was supported in part under the auspices of the University Relations Program at Lawrence Livermore National Laboratory using UCDRD funds and by the US Department of Energy at LLNL under contract W-7405-ENG-48.

REFERENCES

Bonaccini, D., & Tyson, R. K., eds. 1998, Proc. SPIE, 3353
Buscher, D. 1988, MNRAS, 235, 1203
Buscher, D. F., Baldwin, J. E., Warner, P. J., & Haniff, C. A. 1990, MNRAS, 245, 7
Buscher, D. F., & Haniff, C. A. 1993, J. Opt. Soc. Am. A, 10, 1882
Chanan, G., Troy, M., Dekens, F., Michaels, S., Nelson, J., Mast, T., & Kirkman, D. 1998, Appl. Opt., 37, 140
Cornwell, T. J. 1988, Proc. IEEE Trans. Antennas and Propagation, 36, 1165
Danchi, W. C., Tuthill, P. G., Bester, M., Lipman, E. A., Monnier, J. M., & Townes, C. H. 1998, in ASP Conf. Ser. 154, Tenth Cambridge Workshop on Cool Stars, Stellar Systems, and the Sun, ed. R. A. Donahue & J. A. Bookbinder (San Francisco: ASP), 361
Fizeau, H. 1868, Comptes Rendus de l'Académie des Sciences, 66, 932
Golay, M. J. E. 1970, J. Opt. Soc. Am., 61, 272
Gull, S. F., & Skilling, J. 1984, Proc. IEEE, 131, 6
Haniff, C. A., & Buscher, D. F. 1992, J. Opt. Soc. Am. A, 9, 203
Haniff, C. A., Mackay, C. D., Titterington, D. J., Sivia, D., & Baldwin, J. E. 1987, Nature, 328, 694
Hardy, J. W. 1998, Adaptive Optics for Astronomical Telescopes (Oxford Series in Optical and Imaging Sciences 16; New York: Oxford Univ. Press)
Högbom, J. 1974, A&AS, 15, 417
Jennison, R. C. 1958, MNRAS, 118, 276
Keto, E. 1997, ApJ, 475, 843
Labeyrie, A. 1970, A&A, 6, 85
Lohmann, A. W., Weigelt, G., & Wirnitzer, B. 1983, Appl. Opt., 22, 4028
Matthews, K., Ghez, A. M., Weinberger, A. J., & Neugebauer, G. 1996, PASP, 108, 615
Michelson, A. A. 1890, Philos. Mag., 30, 1
Monnier, J. D. 1999, Ph.D. thesis, Univ. California, Berkeley
Monnier, J. D., Tuthill, P. G., & Danchi, W. C. 1999, ApJ, 525, L97
Monnier, J. D., Tuthill, P. G., Danchi, W. C., & Haniff, C. 1997, AAS Meeting, 191, 114.05
Monnier, J. D., Tuthill, P. G., Lopez, B., Cruzalebes, P., Danchi, W. C., & Haniff, C. A. 1999a, ApJ, 512, 351
Negrete-Regagnon, P. 1996, J. Opt. Soc. Am., 13, 1557
Patience, J., Ghez, A. M., Reid, I. N., Weinberger, A. J., & Matthews, K. 1998, AJ, 115, 1972
Readhead, A. C. S., Nakajima, T. S., Pearson, T. J., Neugebauer, G., Oke, J. B., & Sargent, W. L. W. 1988, AJ, 95, 1278
Roddier, F. 1987, J. Opt. Soc. Am. A, 4, 1396
Roddier, F., ed. 1999, Adaptive Optics in Astronomy (Cambridge: Cambridge Univ. Press)
Sivia, D. S. 1987, Ph.D. diss., Cambridge Univ.
Troy, M., Chanan, G. A., Sirko, E., & Leffert, E. 1998, Proc. SPIE, 3352, 307
Tuthill, P. G., Danchi, W. C., Hale, D. D. S., Monnier, J. D., & Townes, C. H. 2000, ApJ, in press
Tuthill, P. G., Haniff, C. A., & Baldwin, J. E. 1999a, MNRAS, 306, 353

Tuthill, P., Monnier, J., & Danchi, W. 1998a, in ASP Conf. Ser. 135, A Half Century of Stellar Pulsation Interpretation: A Tribute to Arthur N. Cox, ed. P. A. Bradley & J. A. Guzik (San Francisco: ASP), 322
———. 1999b, Nature, 398, 487
———. 1999c, in ASP Conf. Ser. 194, Working on the Fringe: An International Conference on Optical and IR Interferometry from Ground and Space, Dana Point, CA, May 24-27, ed. S. Unwin & R. Stachnik (San Francisco: ASP), 54
Tuthill, P. G., Monnier, J. D., Danchi, W. C., & Haniff, C. A. 1998b, Proc. SPIE, 3350, 839
———. 1998c, in ASP Conf. Ser. 154, The Tenth Cambridge Workshop on Cool Stars, Stellar Systems and the Sun, ed. R. A. Donahue & J. A. Bookbinder (San Francisco: ASP), 2057
van Belle, G. T., et al. 1999, AJ, 117, 521
Weigelt, G. 1991, in Progress in Optics 29, ed. E. Wolf Amsterdam: Elsevier), 293
Weigelt, G., Balega, Y., Blocker, T., Fleischer, A. J., Osterbart, R., & Winters, J. M. 1998, A&A, 333, L51
Wilson, R. W., Dhillon, V. S., & Haniff, C. A. 1997, MNRAS, 291, 819